INTERNATIONAL JOURNAL FOR NUMERICAL METHODS IN FLUIDS, VOL. 24, 1091–1110 (1997)

FINITE ELEMENT COMPUTATIONS FOR UNSTEADY FLUID AND ELASTIC MEMBRANE INTERACTION PROBLEMS

S.-J. LIANG,[1]* G. P. NEITZEL[1]† AND C. K. AIDUN[2]

[1] *The George W. Woodruff School of Mechanical Engineering, Georgia Institute of Technology, Atlanta, GA 30332-0405, U.S.A.*
[2] *Institute of Paper Science and Technology, 500 10th Street NW, Atlanta, GA 30318-5794, U.S.A.*

SUMMARY

The interaction between the hydrodynamic forces of a flow field and the elastic forces of adjacent deformable boundaries is described by elastohydrodynamics, a coupled fluid–elastic membrane problem. Direct numerical solution of the unsteady, highly non-linear equations requires that the dynamic evolution of both the flow field and the domain shape be determined as part of the solution, since neither is known *a priori*. This paper describes a numerical algorithm based on the deformable spatial domain space–time (DSD/ST) finite element method for the unsteady motion of an incompressible, viscous fluid with elastic membrane interaction. The unsteady Navier–Stoke and elastic membrane equations are solved separately using an iterative procedure by the GMRES technique with an incomplete lower-upper (ILU) decomposition at every time instant. One-dimensional, two-dimensional and deformable domain model problems are used to demonstrate the capabilities and accuracy of the present algorithm. Both steady state and transient problems are studied. © 1997 by John Wiley & Sons, Ltd.

Int. J. Numer. Meth. Fluids **24**, 1091–1110, 1997.

No. of Figures: 14. No. of Tables: 0. No. of Refs: 47.

KEY WORDS: elastohydrodynamics; fluid–membrane interactions; moving boundary problems; deformable spatial domain/space–time (DSD/ST) finite element method

INTRODUCTION

Flows involving moving boundaries and their associated hydrodynamic instabilities are encountered in many industrial, technological and environmental applications.[1] One such application is in thin film coating systems where a viscous liquid is applied to a flat, deformable substrate such as paper, photographic film or plastic or magnetic tape.[2–5] The ideal mode of fluid flow in most thin film coating systems is two-dimensional, laminar and steady state. Even a small non-uniform deformation of the substrate and/or the coating element due to flow instabilities or flow–elastic interactions could result in a non-uniform coating thickness or other defects. Non-uniform hydrodynamic forces on the

* Current address: National Center for High-Performance Computing, Hsinchu, Taiwan.
† Corresponding author.
Contract grant sponsor: National Science Foundation: Contract grant number: CTS-9258667

CCC 0271–2091/97/111091–20 $17.50 *Received 7 August 1995*

substrate and the likelihood of flow instability increase with the coating application speed. The demands for higher production rate and better quality require higher coating speeds with a laminar, stable, two-dimensional, steady state flow. Our goals are to develop a numerical algorithm to study the coupled fluid–elastic surface interaction and to understand the physics of the associated hydrodynamic instabilities,[6–8] in particular to investigate the *transient* behaviour of the coupled fluid–elastic surface interaction problem.

Many numerical methods have been devised to study moving boundary problems. These include, but are not limited to, the finite difference/finite element arbitrary Lagrangian–Eulerian[9–15] and deformable cell[16] methods as well as the marker-and-cell[17–19] and related volume-of-fluid[20] and boundary element[21–23] methods. Additionally, global mapping of an irregular and changing flow domain to a rectangular space[24,25] on which the standard finite difference/finite volume discretization can be applied has also been successful.[26–28]

The space–time (continuous-in-time) finite element formulation has been successfully applied to various problems with fixed spatial domains.[29–30] The basics of the method, its implementation and the associated stability and accuracy analyses can be found in these references. In a parallel development the discontinuous-in-time space–time method[31,32] has been gaining popularity for fixed domain problems as an alternative to the common semidiscrete (finite difference/finite element in space, finite difference in time) approach. Its advantage is that the finite element interpolation functions are discontinuous in time so that the fully discrete equations are solved one space–time slab at a time, which makes the computations feasible.

The deformable spatial domain/space–time (DSD/ST) finite element formulation, which was introduced earlier,[35] has been successfully applied for the computation of unsteady flow involving free surfaces and two-liquid interfaces,[36] moving mechanical components[37] and fluid–structure[38] and fluid–particle[39] interactions. In the original DSD/ST method the stabilized finite element formulation of the governing equations is written over the space–time domain of the problem and therefore the deformation of the spatial domain with respect to time is automatically taken into account. With the advanced stabilization techniques[33,34] used in the original DSD/ST formulation, the numerical stability problems which are sometimes encountered are overcome with minimal numerical dissipation and therefore with minimal loss of accuracy.

In this study a numerical algorithm based on the deformable spatial domain/space–time (DSD/ST) finite element method is employed to study the fluid–membrane interaction problem. We do not include the stabilization techniques used in the original DSD/ST method, since the main focus of the current study is on devising a numerical scheme to study the fluid–membrane interaction and problems thus considered are generally not convection-dominated flows. Similar studies for the steady state fluid–membrane interaction employing the finite element method[40,41] and finite volume method[42] have been reported recently.

GOVERNING EQUATIONS AND BOUNDARY CONDITIONS

The equations governing the dynamics of an incompressible, viscous fluid bounded by an elastic membrane are outlined in the following.

The Navier–Stokes equations

We consider an incompressible, viscous fluid occupying at an instant $t \in [0, T_\infty]$ a bounded region Ω_t in $\mathbb{R}^{n_{sd}}$, with boundary Γ_t, where n_{sd} is the number of space dimensions. The Navier–Stokes

equations which describe the flow of an unsteady, imcompressible Newtonian fluid with constant properties, written in terms of primitive variables, are

$$\rho_{\mathrm{l}}\left(\frac{\partial \mathbf{u}}{\partial t}+\mathbf{u}\cdot\nabla\mathbf{u}\right)-\nabla\cdot\sigma=0, \tag{1}$$

$$\nabla\cdot\mathbf{u}=0 \quad \text{on } \Omega_t, \quad \forall t\in[0,T_\infty], \tag{2}$$

where $\rho_{\mathrm{l}}(\mathbf{x},t), \mathbf{u}(\mathbf{x},t), p(\mathbf{x},t)$ and $\sigma(\mathbf{x},t)$ are the density, velocity, pressure and stress tensor respectively and the spatial and temporal co-ordinates are denoted by $\mathbf{x}$ and t respectively. The stress tensor is written as the sum of its isotropic and deviatoric parts:

$$\sigma=-p\mathbf{I}+2\mu\varepsilon(\mathbf{u}), \tag{3}$$

with

$$\varepsilon(\mathbf{u})=\tfrac{1}{2}[\nabla\mathbf{u}+(\nabla\mathbf{u})^{\mathrm{T}}], \tag{4}$$

where μ represents the fluid dynamic viscosity and $\mathbf{I}$ denotes the identity tensor.

The momentum equation boundary conditions which are commonly employed may be classified as either the specification of velocity components (Dirichlet type),

$$\mathbf{u}=\mathbf{g} \quad \text{on } (\Gamma_t)_{\mathrm{g}}, \tag{5}$$

or the specification of surface stresses (Neumann type),

$$\sigma\cdot\mathbf{n}=\mathbf{h} \quad \text{on } (\Gamma_t)_{\mathrm{h}}, \tag{6}$$

where $\mathbf{n}$ is the outward unit normal vector to the boundary and $(\Gamma_t)_{\mathrm{g}}$ and $(\Gamma_t)_{\mathrm{h}}$ are complementary subsets of the boundary Γ_t.

The initial condition consists of the specification of velocity, $\mathbf{u}(\mathbf{x},0)=\mathbf{u}_0$. The initial velocity field $\mathbf{u}_0$ is assumed to be solenoidal, i.e.

$$\nabla\cdot\mathbf{u}_0=0 \quad \text{on } \Omega_0. \tag{7}$$

The elastic membrane equation

The membrane equation describing the deformable boundary $(\tilde{\Gamma}_t)_{\mathrm{g}}\in(\Gamma_t)_{\mathrm{g}}$, is given as

$$\rho_{\mathrm{m}}\frac{\mathrm{d}^2\delta}{\mathrm{d}t^2}-\tilde{T}\kappa+\frac{\mathrm{d}^2}{dx^2}(EI\ \kappa)=\sigma \quad \text{on } x_{\mathrm{L}}\leqslant x\leqslant x_{\mathrm{R}}, \quad \forall t\in[0,T_\infty], \tag{8}$$

with boundary conditions

$$\delta|_{x=x_{\mathrm{L}}}=\delta_{\mathrm{L}}, \qquad \delta|_{x=x_{\mathrm{R}}}=\delta_{\mathrm{R}}, \qquad EI\ \kappa|_{x=x_{\mathrm{L}}}=M_{x_{\mathrm{L}}}, \qquad EI\ \kappa|_{x=x_{\mathrm{R}}}=M_{x_{\mathrm{R}}}, \tag{9}$$

where ρ_{m} is the mass per unit area, $\tilde{T}$ is the tension per unit length, E is the modulus of elasticity, I is the second moment of area, σ is the hydrodynamic force per unit area, δ is the displacement of the elastic membrane, M is the bending moment and the curvature $\kappa(x)$ is defined as

$$\kappa(x)=\frac{\mathrm{d}^2\delta/\mathrm{d}x^2}{[1+(\mathrm{d}\delta/\mathrm{d}x)^2]^{3/2}}. \tag{10}$$

As initial conditions, displacements and velocities at $t=0$ are specified for the membrane:

$$\delta(t=0)=\delta_0, \qquad \dot{\delta}(t=0)=\dot{\delta}_0, \tag{11}$$

where the overdot denotes the time derivative.

FINITE ELEMENT FORMULATION

The formulation of the DSD/ST finite element method without including the stabilization technique is outlined in the following. A detailed description of the DSD/ST finite element method and its applications can be found in References 31 and 35.

In order to construct the finite element function spaces for the DSD/ST method, we partition the computation time interval $[0, T_\infty]$ into subintervals $I_n =]t_n, t_{n+1}[$, where t_n and t_{n+1} belong to an ordered series of time levels $0 = t_0 < t_1 < \cdots < t_N < t_{N+1} = T_\infty$. Let $\Omega_n = \Omega_{t_n}$ and $\Gamma_n = \Gamma_{t_n}$. We can define the space–time slab Q_n as the domain enclosed by the surface Ω_n, Ω_{n+1} and P_n, where P_n is the surface described by the boundary Γ_t^h as t travels I_n. P_n is divided into $(P_n)_{\mathrm{g}}$ and $(P_n)_{\mathrm{h}}$ with respect to the type of boundary condition (Dirichlet or Neumann) being applied. For each space–time slab Q_n we define the following finite element interpolation function spaces for velocity and pressure:

$$(S_{\mathbf{u}}^h)_n = \{\mathbf{u}^h | \mathbf{u}^h \in [H^{2h}(Q_n)]^{n_{sd}}, \mathbf{u}^h \approx \mathbf{g}^h \text{ on } (P_n)_{\mathrm{g}}\}, \tag{12}$$

$$(V_{\mathbf{u}}^h)_n = \{\mathbf{u}^h | \mathbf{u}^h \in [H^{2h}(Q_n)]^{n_{\mathrm{sd}}}, \mathbf{u}^h \approx 0 \text{ on } (P_n)_{\mathrm{g}}\}, \tag{13}$$

$$(S_p^h)_n = (V_p^h)_n = \{q^h | q^h \in [H^{1h}(Q_n)]\}. \tag{14}$$

Here $H^{1h}(Q_n)$ and $H^{2h}(Q_n)$ represent the finite-dimensional function space with first- and second-order polynomials in space over the space–time slab Q_n. Over the parent (element) domain this space is formed by using second-order (biquadratic) polynomials for velocity and first-order (bilinear) polynomials for pressure in space and zeroth-order polynomials in time. Globally, the interpolation functions are continuous in space but discontinuous in time.

Equations determining the value of unknowns $\mathbf{u}$ and p are derived using the DSD/ST finite element method. The unsteady Navier–Stokes equations are multiplied by the finite element basis functions and integrated over the space–time slab Q_n. Values of the unknowns are found based on the constraint that the residuals vanish. The DSD/ST formulation for the Navier–Stokes equations can then be written as follows: given $(\mathbf{u}^h)_n^-$, find $\mathbf{u}^h \in (S_{\mathbf{u}}^h)_n$ and $p^h \in (S_p^h)_n$ such that

$$\begin{aligned}
&\int_{Q_n} w^h \cdot \rho_1 \left(\frac{\partial \mathbf{u}^h}{\partial t} + \mathbf{u}^h \cdot \nabla \mathbf{u}^h \right) \mathrm{d}Q + \int_{Q_n} \varepsilon(w^h) : \sigma(p^h, \mathbf{u}^h) \mathrm{d}Q + \int_{Q_n} q^h \nabla \cdot \mathbf{u}^h \mathrm{d}Q \\
&\quad + \int_{\Omega_n} (w^h)_n^+ \cdot \rho_1 [(\mathbf{u}^h)_n^+ - (\mathbf{u}^h)_n^-] \mathrm{d}\Omega \\
&\quad = \int_{(P_n)_{\mathrm{h}}} w^h \cdot \mathbf{h}^h \mathrm{d}P, \quad \forall \mathbf{w}^h \in (V_{\mathbf{u}}^h)_n, \quad \forall q^h \in (V_p^h)_n.
\end{aligned} \tag{15}$$

This procedure is applied sequentially to all the space–time slabs $Q_1, Q_2, \ldots, Q_N$. In the variational formulation given by (15), the following notation is used:

$$(\mathbf{u}^h)_n^{\pm} \equiv \lim_{\varepsilon \to 0} \mathbf{u}(t_n \pm \varepsilon), \tag{16}$$

$$\int_{Q_n} (\cdots) \, \mathrm{d}Q \equiv \int_{t_n}^{t_{n+1}} \int_{\Omega_t^h} (\cdots) \, \mathrm{d}\Omega \, \mathrm{d}t, \tag{17}$$

$$\int_{P_n} (\cdots) \, \mathrm{d}Q \equiv \int_{t_n}^{t_{n+1}} \int_{\Gamma_t^h} (\cdots) \, \mathrm{d}\Gamma \, \mathrm{d}t. \tag{18}$$

Similarly, the elastic membrane equation is discretized using the DSD/ST finite element formulation with the quadratic basis function $\tilde{w}^h$ as

$$\int_{t_n}^{t_{n+1}} \int_{x_L}^{x_R} \tilde{w}^h \left(\rho_m \frac{d\dot{\delta}^h}{dt} - T\kappa + \frac{d^2}{dx^2}(EI\kappa) - \sigma^h \right) dx\, dt + \int_{t_n}^{t_{n+1}} \int_{x_L}^{x_R} (\tilde{w}^h)_n^+ \rho_m [(\dot{\delta}^h)_n^+ - (\dot{\delta}^h)_n^-]\, dx\, dt = 0. \tag{19}$$

Since zeroth-order polynomials in time are employed in the computations, the first term in (19) vanishes and the jump term represented by the second integral behaves like a backward Euler scheme. The location of the membrane is updated using the relation

$$\delta_{n+1}^h = \delta_n^h + \frac{\Delta t}{2}(\dot{\delta}_n^h + \dot{\delta}_{n+1}^h). \tag{20}$$

The Navier–Stokes and elastic membrane equations are solved sequentially and converge iteratively (decoupled) on a solution that satisfies both for every time instant. In this approach the fluid and the elastic membrane have to exchange information concerning the boundaries at the interface. The fluid solver transmits to the membrane solver the hydrodynamic force (resulting from the fluid action) at the interface. In return, the membrane solver transmits the information concerning the interface displacement (resulting from the elastic membrane response to the hydrodynamic force). The resulting system of equations, $\mathbf{Ax} = \mathbf{b}$, is solved by the GMRES technique[43] with an incomplete lower-upper (ILU) decomposition. The computations start with initial conditions

$$(u^h)_0^- \equiv u_0, \qquad (\delta^h)_0^- \equiv \delta_0, \qquad (\dot{\delta}^h)_0^- \equiv \dot{\delta}_0^h, \tag{21}$$

initial domain Ω_0 and initial boundary conditions $(\Gamma_0)_g$, $(\Gamma_0)_h$ and $(\tilde{\Gamma}_0)_g$.

NUMERICAL EXAMPLES

The following numerical examples are presented to demonstrate the capability and accuracy of the DSD/ST finite element method and its application to fluid–membrane interactions.

One-dimensional wave equation

The one-dimensional, unsteady, pure convection problem with constant convection velocity u is

$$\frac{\partial T}{\partial t} + u\frac{\partial T}{\partial x} = 0 \quad \text{on } \Omega_t = [x_L, x_R], \quad \forall t \in [0, T_\infty], \tag{22}$$

with boundary conditions

$$T(x_L, t) = 1, \qquad T(x_R, t) = 0. \tag{23}$$

The initial condition is a discontinuity spread across one spatial element:

$$T(x, 0) = \begin{cases} 1 & \text{for } x_L \leqslant x \leqslant 0{\cdot}4, \\ 0 & \text{otherwise.} \end{cases} \tag{24}$$

A comparison of the conventional method (finite element in space, finite difference in time) and the DSD/ST finite element method is performed. Computed results with 100 uniform, linear elements and $\Delta t = 0{\cdot}01$ are given in Figure 1 for both methods. With the conventional method (fixed mesh) the discontinuity becomes smoother with increasing time owing to numerical diffusion, as shown in Figure 1(a). The effect of reflection on the left open boundary is also noticeable. However, with the

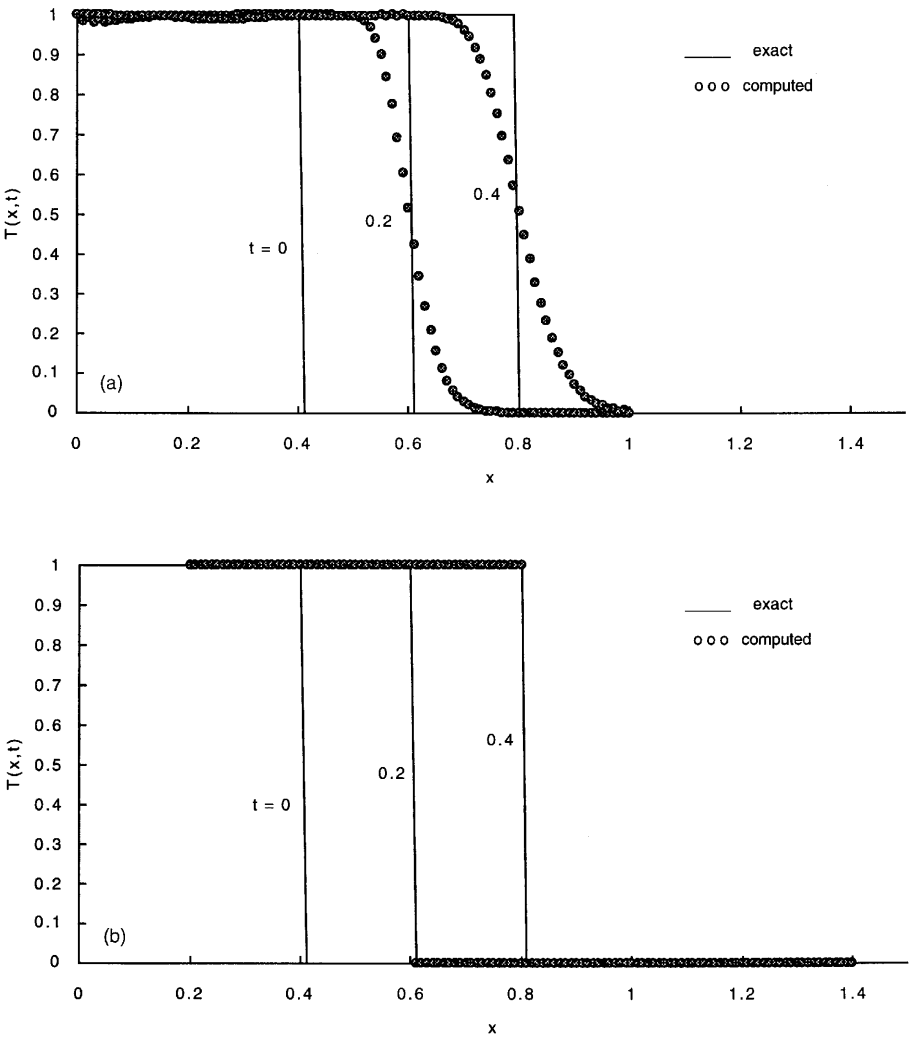

Figure 1. One-dimensional convection of a discontinuity: initial condition and solutions at $t = 0{\cdot}2$ and $0{\cdot}4$ employing (a) conventional (fixed mesh) and (b) DSD/ST (moving mesh) methods

DSD/ST method the mesh is moved with the convection velocity u, the local convection effect (relative to the mesh) is minimized and the exact solution is obtained, as shown in Figure 1(b).

Impulsive plane Couette flow and Stokes plate flow

To assess the accuracy of the DSD/ST finite element method, both an impulsive plane Couette flow (approaching ultimate steady state) and a Stokes plate oscillating flow (a periodic flow) are studied.

Transient Couette flow between two flat, parallel walls. The transient, developing flow between two flat, parallel walls started from rest by the lower wall being impulsively set in motion with

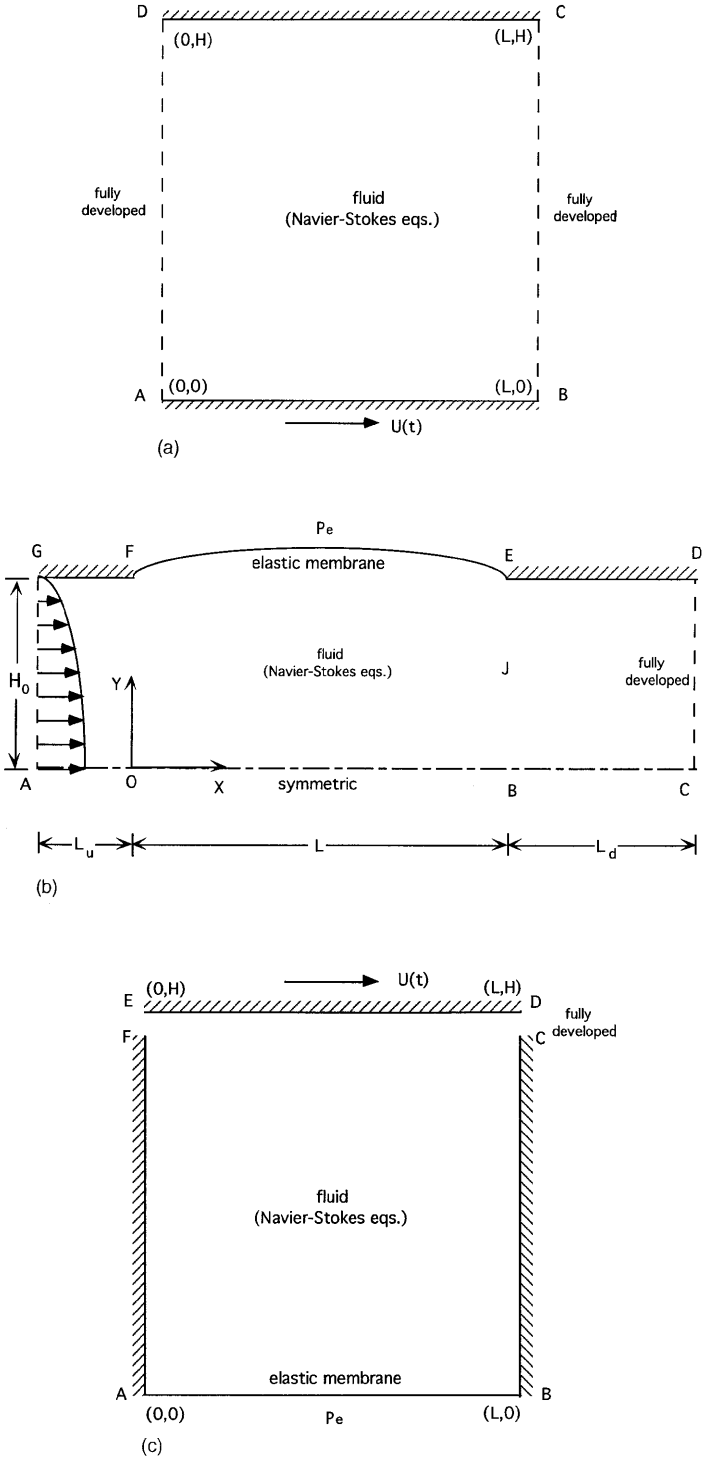

Figure 2. Schematic representation of model problems for (a) impulsive plane Couette flow and Stokes plate flow, (b) a collapsible channel and (c) fluid–membrane interaction

constant speed at $t = 0$ is the impulsive plane Couette flow of interest here. Since the convection terms vanish and the pressure is constant in the whole domain, the momentum equation for the first velocity component $u(y, t)$ simplifies to the diffusion equation

$$\frac{\partial u}{\partial t} = \frac{\partial^2 u}{\partial y^2}, \tag{25}$$

with the second component $v(y, t)$ vanishing identically.

On a two-dimensional unit square domain as illustrated in Figure 2(a), the associated boundary and initial components adopted are

$$u(0, t) = 1, \qquad u(1, t) = 0, \qquad u(y, 0) = 0. \tag{26}$$

This problem admits an infinite series solution[44] of the form

$$u(y, t) = 1 - y - 2 \sum_{n=1}^{\infty} \frac{1}{n\pi} \exp(-n^2 \pi^2 t) \sin(n\pi y). \tag{27}$$

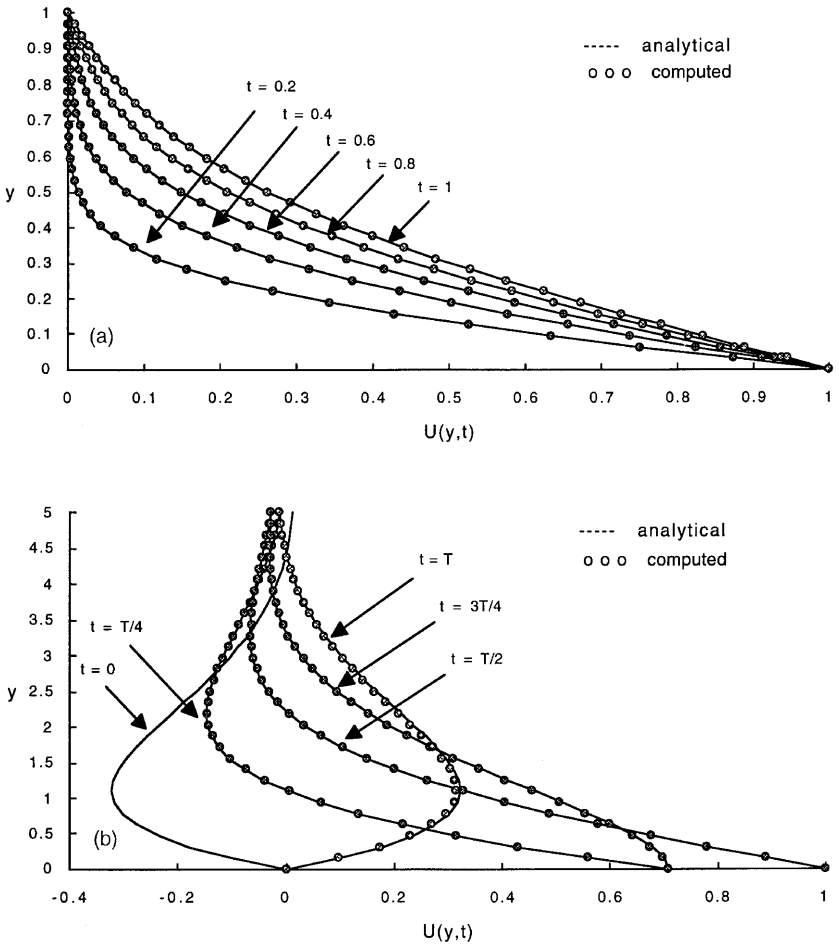

Figure 3. Comparison of analytical solutions with computed solutions for (a) impulsive plane Couette flow and (b) Stokes oscillating plate flow with oscillation period of 2T

A uniform mesh size of 3×33 with constant $\Delta t = 0{\cdot}001$ is employed to solve this problem. Fully developed conditions, i.e. $\partial u/\partial x = 0$, are enforced on $\overline{\mathrm{DA}}$ and $\overline{\mathrm{BC}}$. The computed results are in excellent agreement with the analytical solutions as presented in Figure 3(a).

Stokes oscillating flow between two flat, parallel walls. The Stokes oscillating flow for a semi-infinite fluid at rest initially and bounded below by a solid plate at $y = 0$ is also computed. The problem is to find the periodic motion of the fluid as the lower plate oscillates with $u(0, t) = \sin t$.

The exact solution of Stokes flow for the semi-infinite domain,[44]

$$u(y, t) = \exp(-y/\sqrt{2}) \sin(t - y/\sqrt{2}), \tag{28}$$

is used to establish the boundary and initial conditions for the truncated domain, a finite rectangular domain with $0 \leqslant x \leqslant 1$ and $0 \leqslant y \leqslant 5$, as shown in Figure 2(a). A uniform mesh size of 3×33 with constant $\Delta t = \pi/64$ is employed to solve this problem. Fully developed conditions are enforced on $\overline{\mathrm{DA}}$ and $\overline{\mathrm{BC}}$, as before. The computed results agree well with the analytic solutions as presented in Figure 3(b).

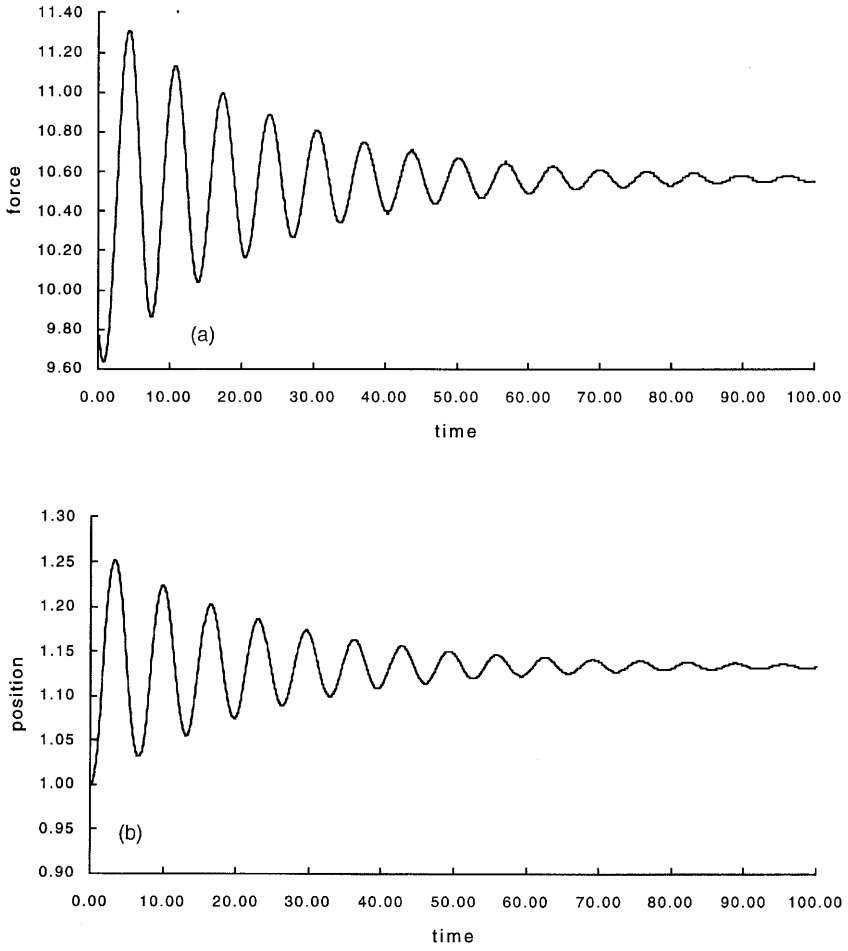

Figure 4. Time histories of (a) hydrodynamic force and (b) position of membrane at $x = 1$ for collapsible channel problem

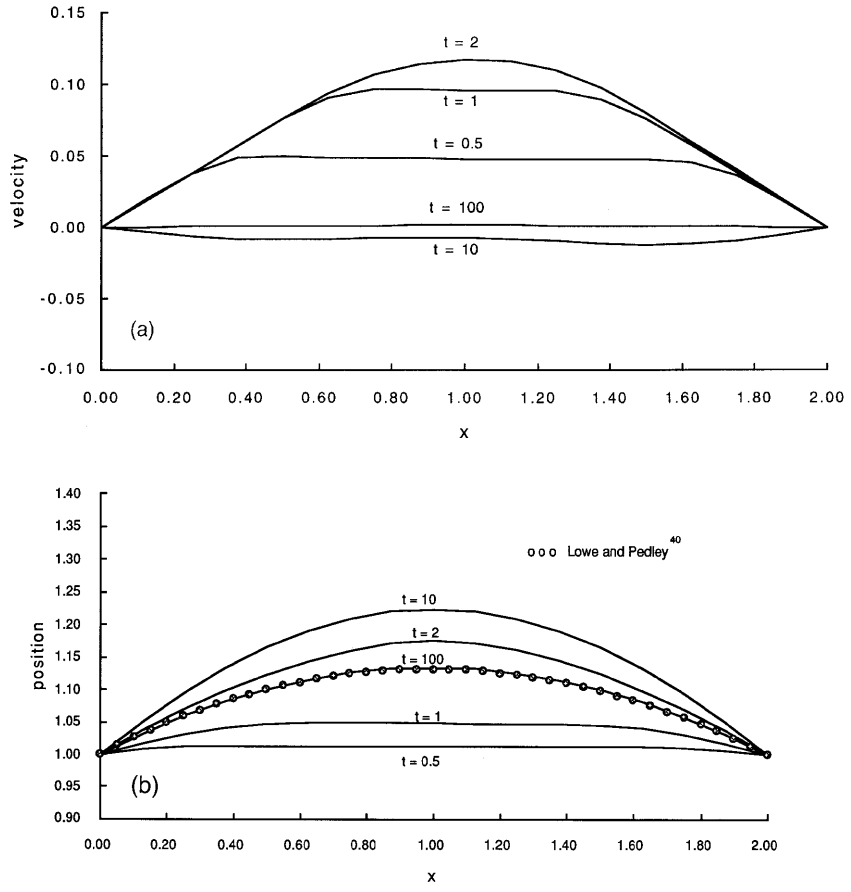

Figure 5. Membrane (a) velocity and (b) shape at selected times for collapsible channel problem

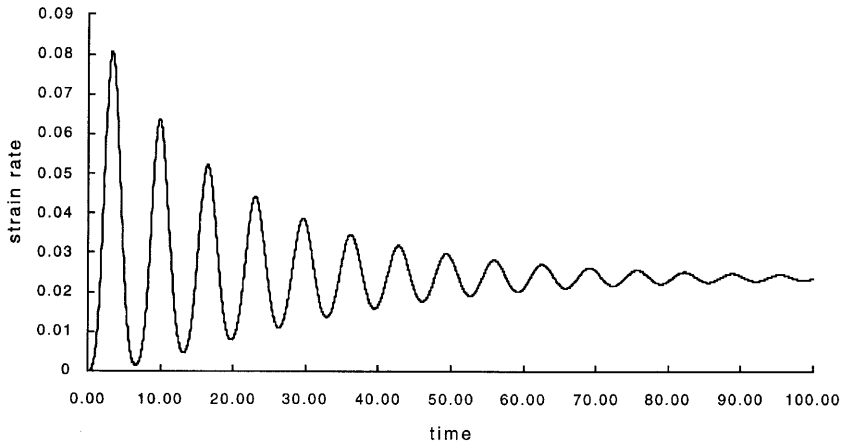

Figure 6. Time history of strain rate of elastic membrane for collapsible channel problem

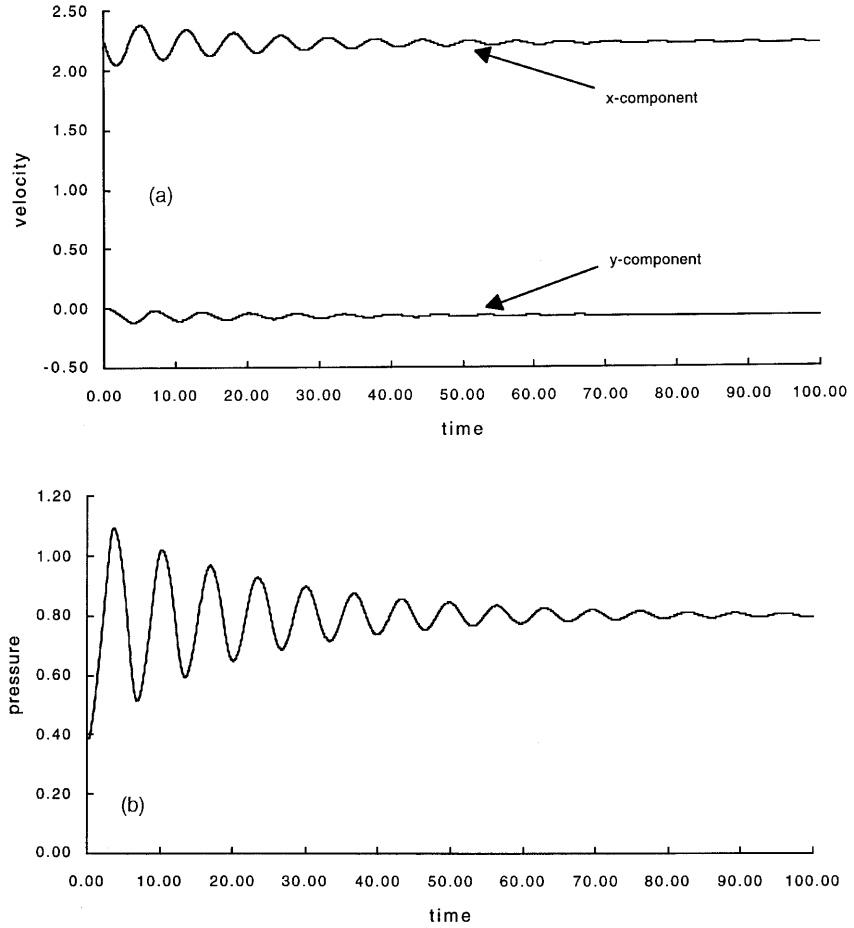

Figure 7. Time histories of (a) velocity and (b) pressure at $(x, y) = (2, 0{\cdot}5)$ for collapsible channel problem

Fluid-membrane interactions

The method is first verified against a lubrication theory solution[45] of a collapsible channel problem (approaching ultimate steady state) and then applied to a fluid–membrane interaction problem with sinusoidal forcing (time-dependent).

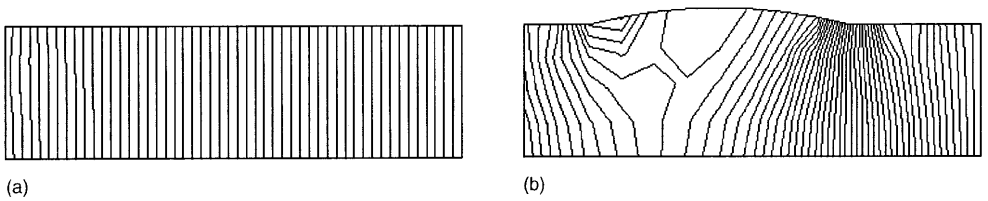

Figure 8. Pressure field at initial condition and near steady state for collapsible channel problem: (a) $t = 0$ ($p_{\min} = 0$, $p_{\max} = 2{\cdot}026$, 50 contours); (b) $t = 100$ ($p_{\min} = 0, p_{\max} = 1{\cdot}845$, 50 contours)

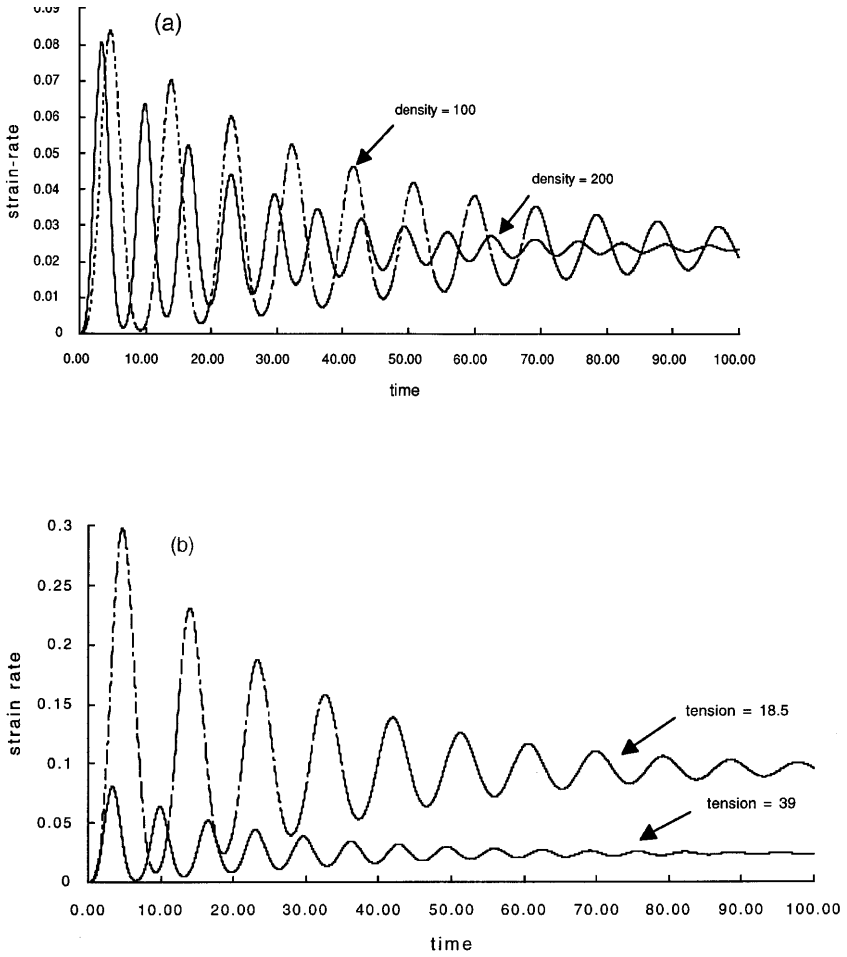

Figure 9. Effects of membrane (a) density and (b) tension on strain rate for collapsible channel problem

Steady state case. A channel with a collapsible segment, as shown in Figure 2(b), is investigated. Only half of the domain is considered, since the problem is symmetric with respect to the centre of the channel. The steady state solution of the problem has been studied using a finite element method with both a streamfunction–vorticity formulation[40] and a primitive variable formulation.[41]

The inflow is taken to be plane Poiseuille flow with an inflow rate Q and hence a parabolic velocity profile is imposed across $\overline{AG}$. At the downstream end of the channel, $\overline{CD}$, a fully developed boundary condition is applied. The membrane $\overline{FE}$ is simply supported at both ends, i.e. both the deflection and bending moment vanish, so that $\delta(x_L = 0) = \delta(x_R = L) = 0$ and $M(x_L = 0) = M(x_R = L) = 0$. The shape of the membrane is unknown *a priori* and must be determined as part of the solution. A channel with $H_0 = 2, L_u = 1, L = 4$ and $L_d = 2$ is assumed. The parameters used for the computation are $\rho_l = 1, \mu = 0{\cdot}1, \rho_m = 100, \tilde{T} = 38, EI = 0, P_e = -9$ and $Q = 1$. The resulting Reynolds number is $Re \equiv \rho u_{avg} H_0/\mu = 20$. A mesh size of 29×9 with constant $\Delta t = 0{\cdot}05$ is employed for this problem. The computation begins from an initial state which assumes an undeformed wall and plane Poiseuille flow.

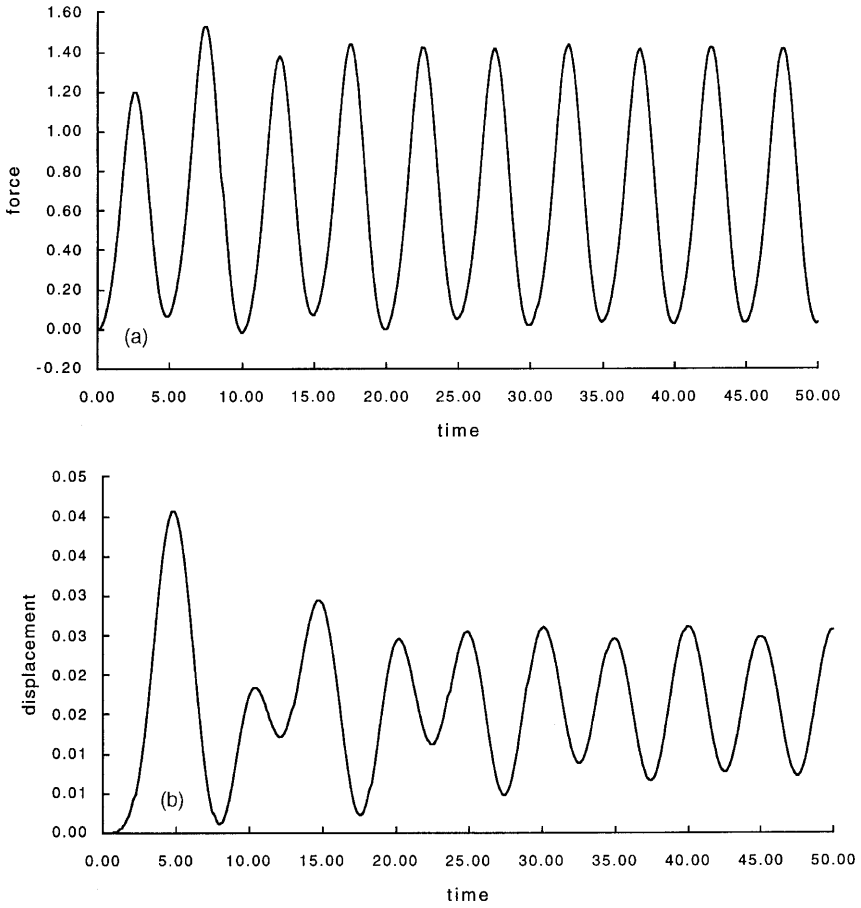

Figure 10. Time histories at $x = 0{\cdot}5$ of (a) hydrodynamic force and (b) displacement of membrane with harmonic forcing

Figures 4(a) and 4(b) present the time histories of the hydrodynamic force and position of the membrane respectively at the centre of the elastic membrane, i.e. $x = 1$. The velocity and shape of the membrane at selected times are presented in Figure 5. The shape of the membrane approaches steady state *non-monotonically*. At steady state the acceleration is zero. The tension of the membrane balances the hydrodynamic force acting on it and hence determines the shape of the membrane from the elastic membrane equation (8). The steady state shape of the membrane is not exactly symmetric with respect to the centre of the membrane. It agrees well with the prediction obtained by the lubrication theory solution,[45] which falls almost exactly on the numerical solution for $t = 100$ (nearly steady state), as shown in Figure 5(b).

The strain rate $\tilde{\varepsilon}(t)$, defined as

$$\tilde{\varepsilon}(t) = \frac{L(t) - L(t=0)}{L(t=0)} = \frac{L_t - L_0}{L_0} = \frac{1}{L_0}\left\{\int_{X_L}^{X_R} \sqrt{\left[1 + \left(\frac{\mathrm{d}y}{\mathrm{d}x}\right)^2\right]}\,\mathrm{d}x - L_0\right\}, \tag{29}$$

is a 'global' measurement of the response of the elastic membrane. The time history of the strain rate is given in Figure 6. Figure 7 presents the time histories of the velocity components and pressure at

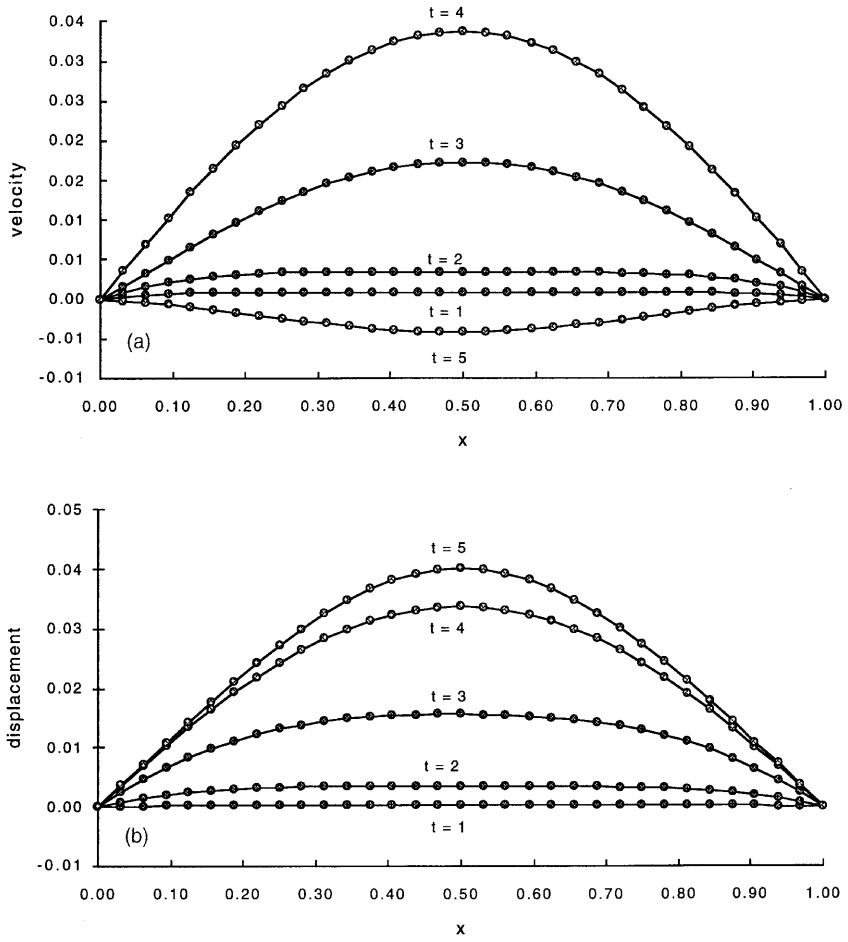

Figure 11(a,b). Membrane (a) velocity and (b) shape at early times of fluid–membrane interaction with harmonic forcing

$(x, y) = (2, 0{\cdot}5)$, point J shown in Figure 2(b). All the quantities presented, both for the elastic membrane and the fluid, demonstrate a *non-monotonic* response during the transition period and approach an ultimate steady state asymptotically. This oscillatory response results mainly from the inertia of the membrane and the non-linearity of the fluid–membrane interactions. The pressure fields at $t = 0$ (the initial condition) and $t = 100$ (nearly steady state) are given in Figure 8. The quantities vary smoothly over the entire domain. The singularity of the pressure field which occurs when using the streamfunction–vorticity formulation[40] is not present, demonstrating clearly the superiority of the primitive variable formulation. Choosing the proper formulation, therefore, is a vital factor for a problem where the accurate pressure solution is required. In this case, for example, the pressure affects the shape of the elastic membrane, which in turn affects the velocity field separately from the direct influence of pressure.

The effects of the density and tension of the membrane on the response of the fluid–membrane interactions are also investigated, as presented in Figure 9. In Figure 9(a) the time histories of the strain rate of the membrane with $\rho_m = 100$ and 200 are shown. Both cases reach the same steady

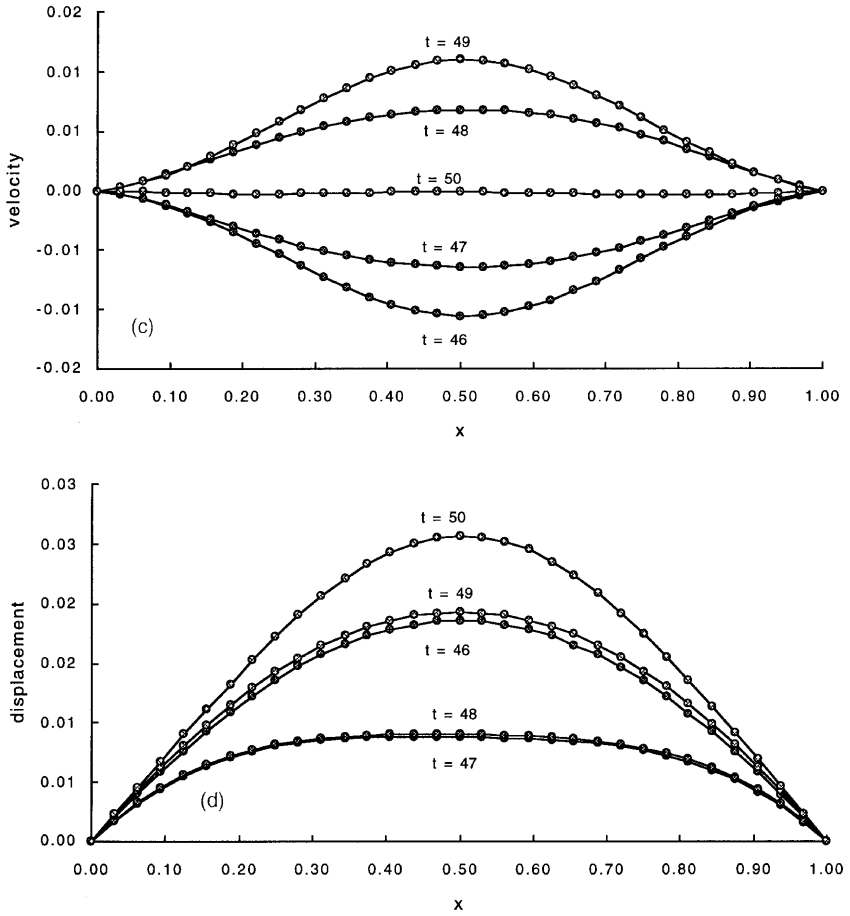

Figure 11(c,d). Membrane (c) velocity and (d) shape at later times of fluid–membrane interaction with harmonic forcing

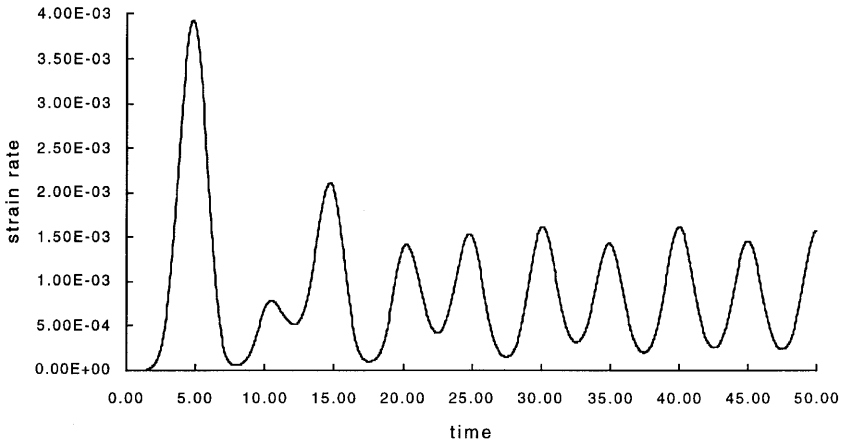

Figure 12. Time history of strain rate of elastic membrane with harmonic forcing

state. The smaller the density of the membrane, the larger are its deformation and inertia and hence the longer it takes for the fluid–membrane system to reach steady state, as expected. The time histories of the strain rate of the membrane with $\tilde{T} = 39$ and 18·5 are shown in Figure 9(b). The smaller the tension of the membrane, the larger is its deformation and the smaller is its frequency of oscillation. This latter observation agrees with one's intuition and results in Reference 46.

Time-dependent case. The second model problem of fluid–membrane interaction, with only one flexible wall, is represented schematically in Figure 2(c). The initial size of the cavity is unity in both the x- and y-direction. There are two openings, $\overline{\mathrm{CD}}$ and $\overline{\mathrm{EF}}$, each with a length of $1/16$. The membrane $\overline{\mathrm{AB}}$ is simply supported at both ends. The shape and motion of the membrane are unknown *a priori* and must be determined as part of the solution. The fluid–membrane interaction is initiated by the motion of the top plate, $u(t)$, and the external applied pressure P_e. On the rigid boundaries $\overline{\mathrm{AB}}, \overline{\mathrm{BC}}, \overline{\mathrm{DE}}$ and $\overline{\mathrm{FA}}$ the no-slip condition is applied, on the open boundary $\overline{\mathrm{CD}}$ a fully developed condition is applied and no boundary condition is applied on $\overline{EF}$.

The parameters used for the computations are $\rho_l = 1, \mu = 0{\cdot}01, \rho_m = 1, \tilde{T} = 1, EI = 0$ and $P_e = 0$. The flow is started by the motion of the top plate in its own plane with speed

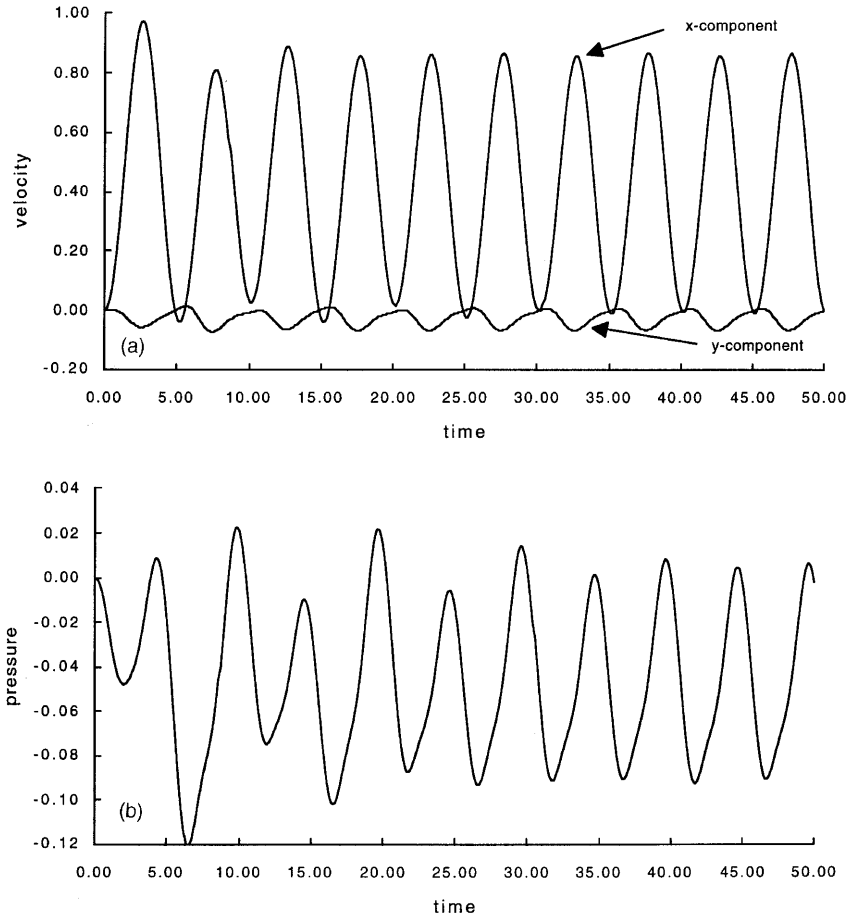

Figure 13. Time histories of (a) velocity and (b) pressure at centre of right exit with harmonic forcing

$u(t) = 1 - \cos(2\pi t/T_f)$, where $T_f = 5$. The resulting Reynolds number is $Re = \mu u_{max} L/\rho_t = 200$. A mesh size of 33×33 with constant $\Delta t = 0{\cdot}05$ is employed. Computed results are presented in Figures 10–14.

Figure 10 shows the time histories of the hydrodynamic force and displacement of the membrane at $x = 0{\cdot}5$. The larger the hydrodynamic force acting on the membrane, the larger is the deformation of the membrane, and *vice versa*. The deformation of the elastic membrane is 180° out-of-phase with the hydrodynamic force acting on it after a period of transition. The velocity distribution and shape of the membrane are given for selected times in Figure 11. After a period of transition the fluid–membrane

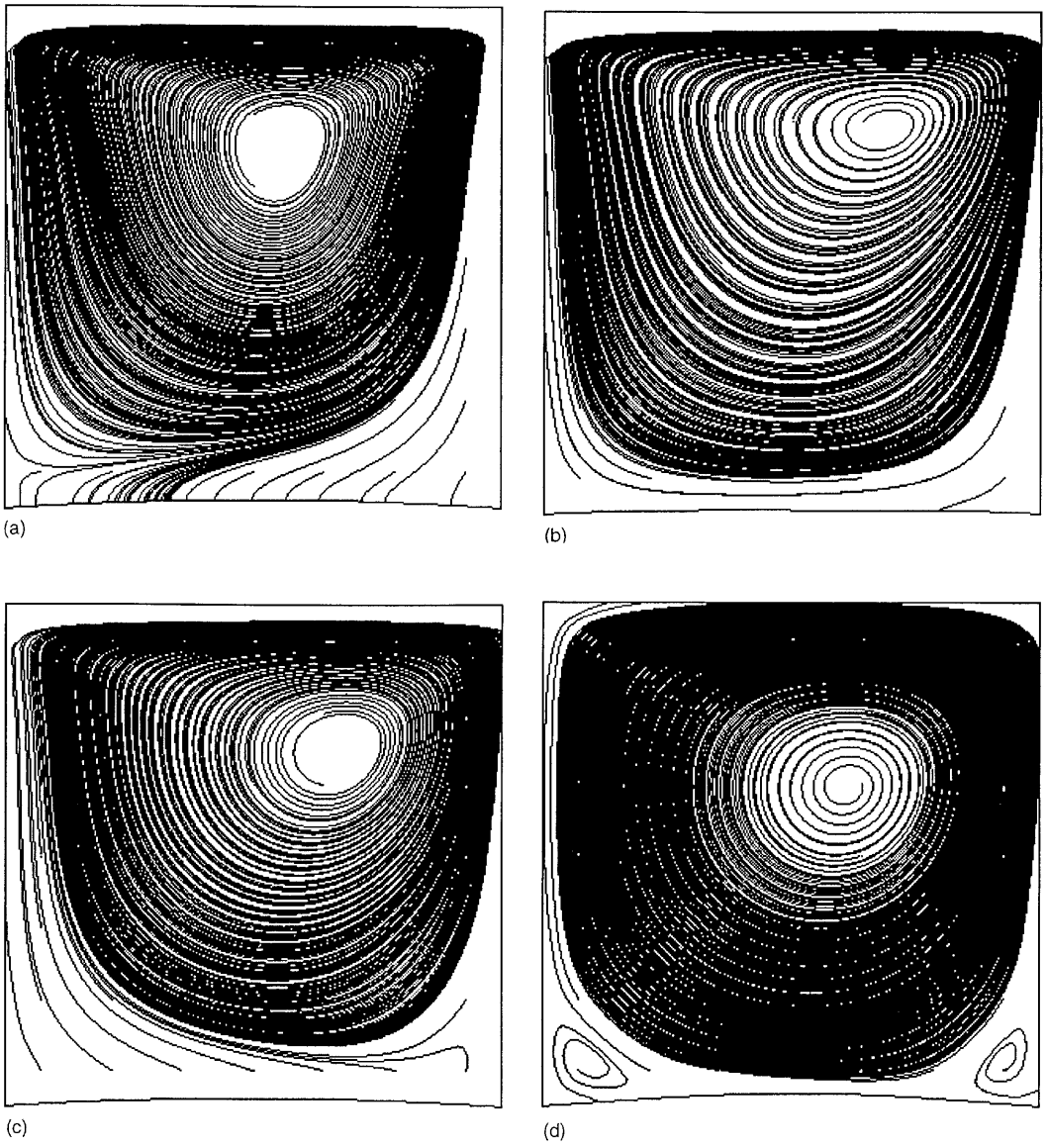

Figure 14. Streamlines with harmonic forcing at times $t =$ (a) 46·25, (b) 47·5, (c) 48·75 and (d) 50

system approaches a periodic response gradually, as demonstrated in Figures 11(c) and 11(d). The time history of the strain rate of the membrane is given in Figure 12 and the time histories of the velocity and pressure at the centre of the right exit are given in Figure 13. Streamlines at $t = 46{\cdot}25, 47{\cdot}5, 48{\cdot}75$ and 50 of the last cycle of the simulation are given in Figure 14. Since the velocities of the membranes are generally not zero, the streamlines intersect with the membrane.

CONCLUSIONS

We employ the deformable spatial domain/space time (DSD/ST) finite element method to study steady and unsteady flows involving moving boundaries. Based on the space–time finite element formulation, the deformation of the spatial domain with respect to time is automatically taken into account. One-dimensional, two-dimensional and deformable domain problems are used to demonstrate the capabilities and accuracy of the present algorithm.

Computed results of the collapsible channel problem (approaching ultimate steady state) show a *non-monotonic* response of the fluid and elastic membrane during the transition period. The inertia of the elastic membrane is found to be important in studying flow-induced vibration problems, as demonstrated Figure 9(a). Using the time-dependent algorithm with no quasi-static assumption for the elastic membrane,[47] we can investigate the transient solution of the fluid–membrane interactions. The steady state solution agrees well with the prediction from lubrication theory.[45] Computed results of the fluid–membrane interaction with harmonic forcing (a periodic flow) show that the fluid–membrane reaches a periodic response after a few cycles of transition. This study constitutes the preparation phase for investigating coupled air–sheet interactions[2,3] and the associated hydrodynamic instabilities.[6–8]

ACKNOWLEDGEMENTS

This work is supported in part by the National Science Foundation (CTS-9258667) and an industrial consortium.

REFERENCES

1. J. M. Crolet and R. Ohayon, *Computational Methods for Fluid–Structure interaction*, Wiley, New York, 1994.
2. A. Pramila, 'Sheet flutter and the interaction between sheet and air', *TAPPI J.*, **69**, 70–74 (1986).
3. Y. B. Chang and P. M. Moretti, 'Interaction of fluttering webs with surrounding air', *TAPPI J.*, **74**, 231–236 (1991).
4. S. F. Kistler and L. E. Scriven, 'Coating flow', in J. R. A. Pearson and S. M. Richardson (eds), *Computational Analysis of Polymer Processing*, Applied Science Publishers, London, 1983, pp. 243–299.
5. K. N. Christoudoulou and L. E. Scriven, 'The fluid mechanics of slide coating', *J. Fluid Mech.*, **208**, 321–354 (1989).
6. C. K. Aidun, 'Principles of hydrodynamic instability: application in coating systems. Part 1: Background', *TAPPI J.*, **74**(2), 213–219 (1991).
7. C. K. Aidun, 'Principles of hydrodynamic instability: application in coating systems. Part 2: Examples of flow instability', *TAPPI J.*, **74**(3), 213–220 (1991).
8. C. K. Aidun, 'Principles of hydrodynamic instability: application in coating systems. Part 3: A generalized view of instability and bifurcation', *TAPPI J.*, **74**(4), 209–213.
9. C. W. Hirt, A. A. Amsden and J. L. Cook, 'An arbitrary Lagrangian–Eulerian computing method for all speeds', *J. Comput. Phys.*, **14**, 227–253 (1974).
10. W. E. Pracht, 'Calculating three-dimensional fluid flows at all speeds with an Eulerian–Lagrangian computing mesh', *J. Comput. Phys.*, **17**, 132–159 (1975).
11. R. K.-C. Chan, 'A generalized arbitrary Lagrangian–Eulerian method for incompressible flows with sharp interfaces', *J. Comput. Phys.*, **17**, 311–331 (1975).
12. T. J. R. Hughes, W. K. Liu and T. K. Zimmermann, 'Lagrangian–Eulerian finite element formulation for incompressible viscous flows', *Comput. Methods Appl. Mech. Eng.*, **29**, 329–349 (1981).
13. A. Huerta and W. K. Liu, 'Viscous flow with large free surface motion', *Comput. Methods Appl. Mech. Eng.*, **69**, 277–324 (1988).

14. R. Ramaswamy and M. Kawahara, 'Arbitrary Lagrangian–Eulerian finite element method for unsteady, convective, incompressible viscous free surface flows', *Int. J. Numer. Methods Fluids*, **7**, 1053–1075 (1987).
15. T. Nomura, 'ALE finite element computations of fluid–structure interaction problems', *Comput. Methods Appl. Mech. Eng.*, **112**, 291–308 (1994).
16. Y. Mizuta, 'Generalized boundary conditions on the basis of a deformable-cell method: free surface, density interfaces and open boundaries', *Comput. Fluids*, **19**, 377–385 (1991).
17. B. J. Daly, 'A technique for including surface tension effects in hydrodynamic calculations', *J. Comput. Phys.*, **4**, 97–117 (1969).
18. R. K.-C. Chan and R. L. Street, 'A computer study of finite amplitude water waves', *J. Comput. Phys.*, **6**, 68–94 (1970).
19. J. A. Viecelli, 'A computing method for incompressible flows bounded by moving walls', *J. Comput. Phys.*, **8**, 119–143 (1971).
20. C. W. Hirt and B. D. Nichols, 'Volume of fluid (VOF) method for the dynamics of free boundaries', *J. Comput. Phys.*, **39**, 201–225 (1981).
21. C. A. Brebbia, *The Boundary Element Method for Engineers*, Pentech, London, 1978.
22. R. I. Tanner, 'Extrudate swell' in J. R. A. Pearson and S. M. Richardson (eds.), *Computational Analysis of Polymer Processing*, Applied Science Publishers, London, 1983, pp. 63–138.
23. Y. Yuan and D. B. Ingham, 'The numerical solution of viscous flows with a free surface', in L. C. Wrobel and C. A. Brebbia (eds), *Computational Modelling of Free and Moving Boundary Problems*, Computational Mechanics Publications, Southampton, 1991, pp. 325–340.
24. J. F. Thompson and Z. U. A. Warsi, 'Boundary-fitted coordinate systems for numerical solution of partial differential equations—a review', *J. Comput. Phys.*, **47**, 1–108 (1982).
25. G. Ryskin and L. G. Leal, 'Orthogonal mapping', *J. Comput. Phys.*, **50**, 71–100 (1983).
26. G. Ryskin and L. G. Leal, 'Numerical solution of free-boundary problems in fluid mechanics. Part 1. The finite-difference technique', *J. Fluid Mech.*, **148**, 1–17 (1984).
27. G. Ryskin and L. G. Leal, 'Numerical solution of free-boundary problems in fluid mechanics. Part 2. Buoyancy-driven motion of a gas bubble through a quiescent liquid', *J. Fluid Mech.*, **148**, 19–35 (1984).
28. G. Ryskin and L. G. Neal, 'Numerical solution of free-boundary problems in fluid mechanics. Part 3. Bubble deformation in an axisymmetric straining flow', *J. Fluid Mech.*, **148**, 37–43 (1984).
29. H. Nguyen and J. Reynen, 'A space–time least-square finite element scheme for advection–diffusion equations', *Comput. Methods Appl. Mech. Eng.*, **42**, 331–342 (1984).
30. B. C. Bell and K. S. Surana, 'A space–time coupled p-version least squares finite element formulation for unsteady fluid dynamics problems', *Int. J. Numer. Methods Fluids*, **9**, 1115–1135 (1994).
31. T. J. R. Hughes and G. M. Hulbert, 'Space–time finite element methods for elastodynamics: formulations and error estimates', *Comput. Methods Appl. Mech. Eng.*, **66**, 339–363 (1988).
32. C. Johnson, U. Navert and J. Pitkaranta, 'Finite element methods for linear hyperbolic problems', *Comput. Methods Appl. Mech. Eng.*, **45**, 285–312 (1984).
33. T. J. R. Hughes, L. P. Franca and M. Mallet, 'A new finite element formulation for computational fluid dynamics: VI: Convergence analysis of the generalized SUPG formulation for linear time-dependent multi-dimensional advective–diffusive systems', *Comput. Methods Appl. Mech. Eng.*, **63**, 97–112 (1987).
34. T. J. R. Hughes, L. P. Franca and G. M. Hulbert, 'A new finite element formulation for computational fluid dynamics: VIII. 'The Galerkin/least-squares method for advective–diffusion equations', *Comput. Methods Appl. Mech. Eng.*, **73**, 173–189 (1989).
35. T. E. Tezduyar, M. Behr and J. Liou, 'A new strategy for finite element computations involving moving boundaries and interfaces—the deformable-spatial-domain/space–time procedure: I. The concept and the preliminary numerical tests', *Comput. Methods Appl. Mech. Eng.*, **94**, 339–351 (1992).
36. T. E. Tezduyar, M. Behr, S. Mittal and J. Liou, 'A new strategyv for finite element computations involving moving boundaries and interfaces—the deformable-spatial-domain/space–time procedure: II. Computation of free-surface flows, two-liquid flows, and flows with drifting cylinders', *Comput. Methods Appl. Mech. Eng.*, **94**, 353–371 (1992).
37. S. K. Aliabadi and T. E. Tezduyar, 'Space–time finite element computation of compressible flows involving moving boundaries and interfaces', *Comput. Methods Appl. Mech. Eng.*, **107** 209–223 (1993).
38. T. E. Tezduyar, S. K. Aliabadi, M. Behr and S. Mittal, 'Massively parallel finite element simulation of compressible and incompressible flows', *Comput. Methods Appl. Mech. Eng.*, **119** 157–177 (1994).
39. A. A. Johnson and T. E. Tezduyar, 'Mesh generation and update strategies for parallel computation of 3D flow problems' in *Computational Mechanics '95, Proc. Int. Conf. on Computational Engineering Science*, Mauna Lani, HI, 1995.
40. T. W. Lowe and T. J. Pedley, 'Finite element solution of a Stokes flow in a channel with a collapsible segment', in J. M. Crolet and R. Ohayon (eds), *Computational Methods for Fluid–Structure Interaction*, Wiley, New York, 1994, pp. 220–229.
41. M. P. Rast, 'Simultaneous solution of the Navier–Stokes and elastic membrane equations by a finite element method', *Int. j. numer. methods fluids*, **9**, 1115–1135 (1994).
42. R. Smith and W. Shyy, 'A computational model of flexible membrane wings in steady laminar flow', *AIAA J.*, in press.
43. Y. Saad and M. H. Schultz, 'GMRES: a generalized minimal residual algorithm for solving nonsymmetric linear systems', *SIAM J. Sci. Stat. Comput.*, **7**, 856–869 (1986).
44. H. Schlichting, *Boundary-Layer Theory*, 6th edn, McGraw-Hill, New York, 1968.

45. T. J. Pedley, 'Longitudinal tension variation in collapsible channels: a new mechanism for the breakdown of steady flow', *Trans. ASME, J. Biomech. Eng.*, **114**, 60–67 (1992).
46. Y. B. Chang, 'An experimental and analytical study of web flutter', *Ph.D. Thesis*, School of Mechanical and Aerospace Engineering, Oklahoma State University, Stillwater, OK, 1990.
47. R. Smith and W. Shyy, 'Computation of unsteady laminar flow over a flexible two-dimensional membrane wing', *Phys. Fluids*, in press.

